ARL-TN-1026 • Sep 2020

Simulations Involving Combined Ballistic Penetration and Blast

by Charles L Randow

NOTICES

Disclaimers

ARL-TN-1026 • SEP 2020

Simulations Involving Combined Ballistic Penetration and Blast

by Charles L Randow
Weapons and Materials Research Directorate, CCDC Army Research Laboratory

REPORT DOCUMENTATION PAGE					*Form Approved* *OMB No. 0704-0188*
Public reporting burden for this collection of information is estimated to average 1 hour per response, including the time for reviewing instructions, searching existing data sources, gathering and maintaining the data needed, and completing and reviewing the collection information. Send comments regarding this burden estimate or any other aspect of this collection of information, including suggestions for reducing the burden, to Department of Defense, Washington Headquarters Services, Directorate for Information Operations and Reports (0704-0188), 1215 Jefferson Davis Highway, Suite 1204, Arlington, VA 22202-4302. Respondents should be aware that notwithstanding any other provision of law, no person shall be subject to any penalty for failing to comply with a collection of information if it does not display a currently valid OMB control number. **PLEASE DO NOT RETURN YOUR FORM TO THE ABOVE ADDRESS.**					
1. REPORT DATE *(DD-MM-YYYY)* September 2020		**2. REPORT TYPE** Technical Note			**3. DATES COVERED (From - To)** 1 March 2020–31 July 2020
4. TITLE AND SUBTITLE Simulations Involving Combined Ballistic Penetration and Blast					**5a. CONTRACT NUMBER**
					5b. GRANT NUMBER
					5c. PROGRAM ELEMENT NUMBER
6. AUTHOR(S) Charles L Randow					**5d. PROJECT NUMBER** AH80
					5e. TASK NUMBER
					5f. WORK UNIT NUMBER
7. PERFORMING ORGANIZATION NAME(S) AND ADDRESS(ES) CCDC Army Research Laboratory ATTN: FCDD-RLW-PD Aberdeen Proving Ground, MD 21005-5066					**8. PERFORMING ORGANIZATION REPORT NUMBER** ARL-TN-1026
9. SPONSORING/MONITORING AGENCY NAME(S) AND ADDRESS(ES)					**10. SPONSOR/MONITOR'S ACRONYM(S)**
					11. SPONSOR/MONITOR'S REPORT NUMBER(S)
12. DISTRIBUTION/AVAILABILITY STATEMENT Approved for public release; distribution is unlimited.					
13. SUPPLEMENTARY NOTES primary author's email: <charles.l.randow2.civ@mail.mil>.					
14. ABSTRACT This work uses numerical modeling to examine two different target configurations subjected to ballistic penetration and blast. The simulations are idealized since they use simplified geometries at a relatively small scale (in terms of projectile and target size and shape). Observations from these simulations suggest that the relative timing between blast and penetration events plays a critical role in determining whether the addition of blast causes target failure. As a result of this work, a number of questions and potential issues are identified. These may serve as motivation and direction for future studies involving a larger set of conditions as well as the possibility of corresponding experiments.					
15. SUBJECT TERMS blast, penetration, failure, finite element analysis, combined effects					
16. SECURITY CLASSIFICATION OF:			**17. LIMITATION OF ABSTRACT**	**18. NUMBER OF PAGES**	**19a. NAME OF RESPONSIBLE PERSON** Charles L Randow
a. REPORT Unclassified	**b. ABSTRACT** Unclassified	**c. THIS PAGE** Unclassified	UU	26	**19b. TELEPHONE NUMBER (Include area code)** 410-306-1007

Standard Form 298 (Rev. 8/98)
Prescribed by ANSI Std. Z39.18

Contents

List of Figures

1. Introduction

This document contains results from 15 simulations involving a spherical steel penetrator impacting two different steel target configurations. One target configuration consists of a single plate, while the other configuration consists of two plates (each plate being half the thickness of the single-plate target). Eight of these simulations also include a spherical explosive detonated (in air) near the target face. The explosive was chosen such that the resulting blast, without the accompanying ballistic penetration, would have a minimal effect on the targets.

The point of this work is not to focus on the well-known differences between homogeneous and multi-layered targets (i.e., the differences between single-plate and double-plate targets). As would be expected, the double-plate target should provide improved penetration resistance as well as a greater likelihood to crack instead of to plug. Also, since blast loading is minimal in these simulations, the higher stiffness for the single-plate target (relative to the double-plate target) should not be relevant.

Instead, the purpose of this brief study is to consider the effect of combining ballistic penetration and blast, and the two target types are examined to see the effect of different failure mechanisms under combined loading. Results suggest that relative timing between the penetration and blast effect determines whether the target resists the threats (by remaining intact) or fails (through plugging and/or crack-like openings). Therefore, the following conditions should be taken into account: the relative positioning of the target and the threat, the relative time interval between impact and detonation of the explosive, and the overall target geometry and boundary conditions.

A brief description of the materials, geometry, and simulation methodology is presented in Section 2. Section 3 provides a summary of the results and Section 4 includes concluding thoughts and ideas for future work.

2. Model Description

As shown in Fig. 1, the three-dimensional models consist of a 10-mm-diameter spherical projectile, a 203.2-mm-diameter circular target (consisting of two 6.35-mm-thick plates or a single 12.7-mm-thick plate), and a 50-mm-diameter spherical explosive. The projectile is mild steel, the target is a high-strength armor steel, and LF-2XA is used for the explosive. The target with two plates will be referred to as the *double-plate target*, while the target with one thicker plate will be called the *single-plate target*. The relative positions of these components are shown in Fig. 2, where there is an initial 0.83-mm gap between the projectile and the target face, and the explosive center is located 45 mm from the target face. Other than the single-plate versus double-plate targets, the geometry remains the same for all of the simulations. (The entire system was modeled, without taking advantage of symmetry, to better account for the lack of symmetry of failure.)

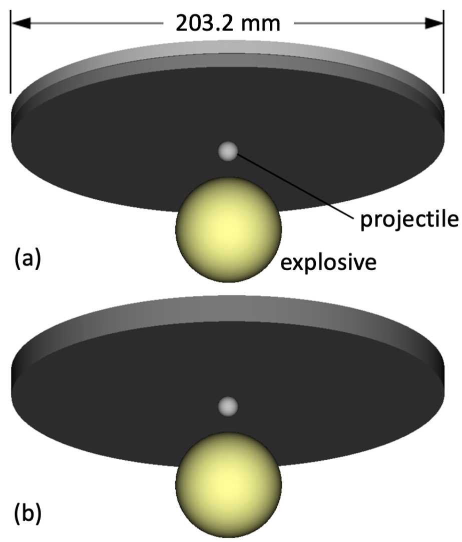

Fig. 1 Explosive, projectile, and target configurations showing a) two 6.35-mm plates (the double-plate target) and b) a single 12.7-mm plate (the single plate target). As shown in the figure, the projectile is traveling upward into the 203.2-mm-diameter target plate(s).

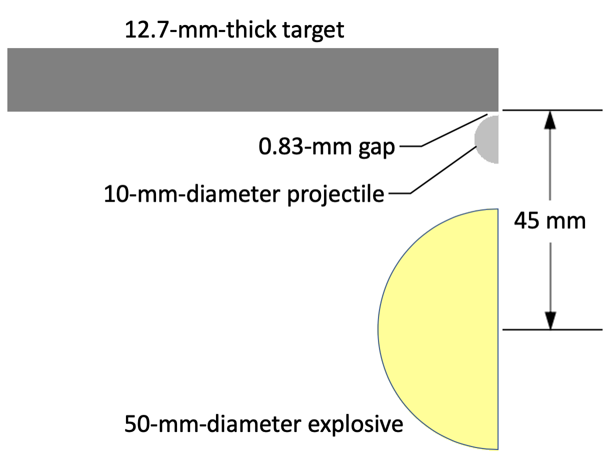

Fig. 2 Side-view (half-symmetric) slice showing overall geometry to illustrate the relative positions of the projectile and explosive to the target face

The projectile was modeled as 1006 alloy steel and the target plates were modeled as rolled homogeneous armor steel. Both steel materials are modeled using the Mie–Gruneisen equation of state[1] and the Johnson–Cook[2] strength and failure models. The same material properties were used for both the 6.35-mm and the 12.7-mm target plates, where the strength parameter A equaled 976.2 MPa. (The variation in strength observed in different thicknesses of this steel[3] were not accounted for in order to limit the number of variables in this work.) For comparison, the same parameter for the mild steel projectile was 350.2 MPa. The explosive was modeled as LF-2XA, using the Jones–Wilkins–Lee equation of state,[4] with a density of 1.75 g/cm^3.

Velodyne,[5] a code with Lagrangian finite element and Eulerian solver capabilities, was used to model the explosive and projectile system. The explosive begins as a Lagrangian part and remains as such after initial detonation until all elements have detonated and significant element distortion has occurred. At this point, the pressure, density, velocity, and internal energy from each Lagrangian element are mapped into the Eulerian background domain. Velodyne also uses smooth particle hydrodynamics for eroded elements, although this approach is not applied to elements of the explosive in these particular models. Solid elements are discarded if they become excessively distorted (e.g., when an element reduces the overall time step below a certain limit or when an element reaches a geometric limit in terms of its Jacobian, relative volume, skew, or aspect ratio). In this work, elements are not discarded due to failure, as defined by the material failure model.

A graded mesh is used for the target plate(s). The centermost 40-mm-diameter region has elements with edge lengths of approximately 0.3 mm, for a total of 714,360 elements. The elements in the remainder of the target gradually increase in size until reaching edge lengths of 1.1–1.6 mm; there are an additional 393,406 elements in this outer part of the target plate(s). The projectile has an average element edge length of 0.3 mm, although edge lengths of 0.48 mm are visible on the outer surface; there are a total of 19,456 elements in the projectile. The explosive is initially treated as a Lagrangian object; it is meshed with an average element edge length of 0.8 mm and there are a total of 15,876 elements. The Eulerian background has overall dimensions of $240 \times 240 \times 120$ mm. The automatic mesh refinement scheme in Velodyne specifies a range of Eulerian cell sizes from 1.25 to 20 mm.

The simulations were run on an SGI ICE XA supercomputer (the Centennial system belonging to the Department of Defense Supercomputing Resource Center) using three nodes. Centennial has two processors per node, and 20 cores per processor, for a total of 120 cores for this work. Each simulation was run out to 90 μs, with the simulations taking approximately 7 h of wall-clock time to run to completion.

3. Simulation Results

The first round of simulations focused on projectile-only interactions, with the goal being to determine an approximate limit velocity for the double-plate and the single-plate targets. The second round of simulations would then investigate the effect of adding blast to targets near the established limit thickness. When including the explosive, the effect of detonation time delay was considered.

An overview of the simulation results (plotting effective plastic strain) for the double-plate target, at a simulation time of 90 μs, is shown in Fig. 3. (These images show the behavior of the entire system; enlarged images showing the central regions for particular examples will be discussed later in this section.) Results for models without explosives and at four different projectile velocities (1800, 2000, 2200, and 2400 m/s) are shown in Figs. 3a, d, h, and i. The effect of a subsequent explosive detonation is also shown in Figs. 3b and c for the 1800-m/s case and in Figs. 3e–g for the 2000-m/s case. It was apparent that for the 1800-m/s case, the explosive would not cause failure in the rear plate, as is evident in Fig. 3c. For the 2400-m/s case, an explosive was not necessary to cause failure in the target, as shown in Fig. 3i.

Therefore, the configuration consisting of a double-plate target and a projectile impact speed of 2000 m/s will be used for a more in-depth analysis; this configuration will be referred to as case A. For case A, fracture occurred with the 5- and 10-μs detonation delays, as shown in Figs. 3f and g, respectively. However, fracture did not occur for the 15-μs delay, as shown in Fig. 3e. And there was also no fracture for the projectile-only case.

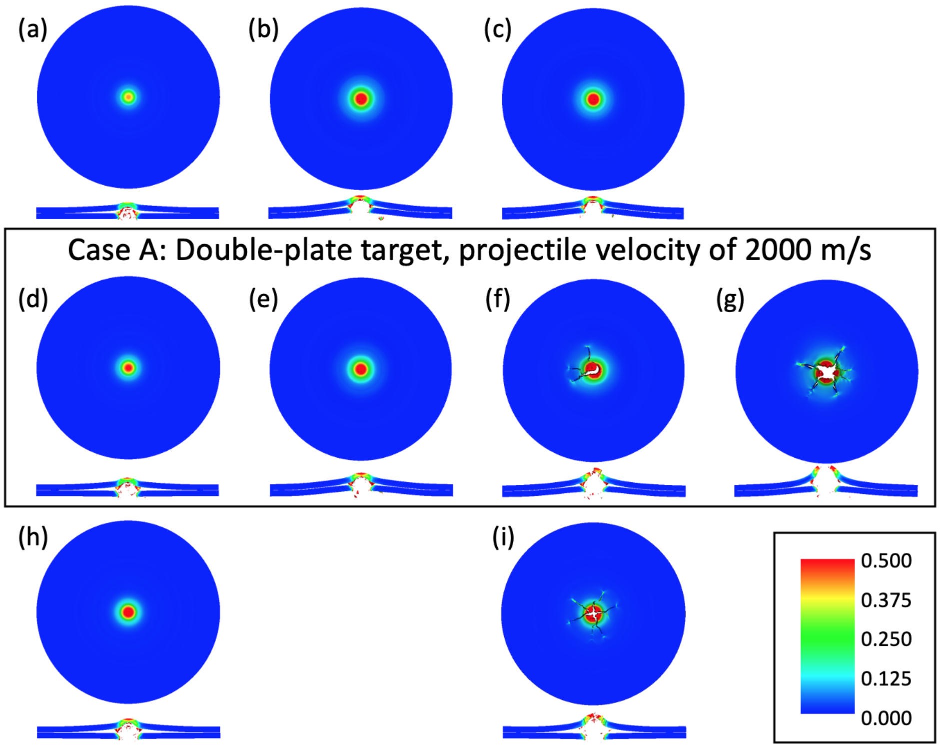

Fig. 3 Images at 90 μs showing effective plastic strain for a variety of two 6.35-mm-thick target plate (double-plate) configurations. A side-view slice and a rear view are included for each configuration with varying projectile velocity and explosive time delay: a) 1800 m/s, no explosive; b) 1800 m/s, 10-μs delay; c) 1800 m/s, 5-μs delay; d) 2000 m/s, no explosive; e) 2000 m/s, 15-μs delay; f) 2000 m/s, 10-μs delay; g) 2000 m/s, 5-μs delay; h) 2200 m/s, no explosive; and i) 2400 m/s, no explosive.

Results at 90 μs for the single-plate target are shown in Fig. 4. The single-plate target fails (through plugging) with a projectile velocity of 2000 m/s, see Fig. 4e. As would be expected, the plug moves farther at a higher velocity with the addition of blast, as shown in Fig. 4f. For the 1800-m/s case, failure through plugging only occurred when the explosive detonation delay was set to 10 μs, as shown in Fig. 4d. Figures 4a–c show varying degrees of damage for the 1800-m/s case with no explosive, with explosive and a 40-μs delay, and with explosive and a 20-μs delay, respectively. Therefore, the 1800-m/s case will be used with the single-plate target for additional analysis, and this will be called case B. Cases A and B are not exact limit thicknesses for their corresponding projectile velocities, but they do show the transition to target failure with blast (under certain timing conditions).

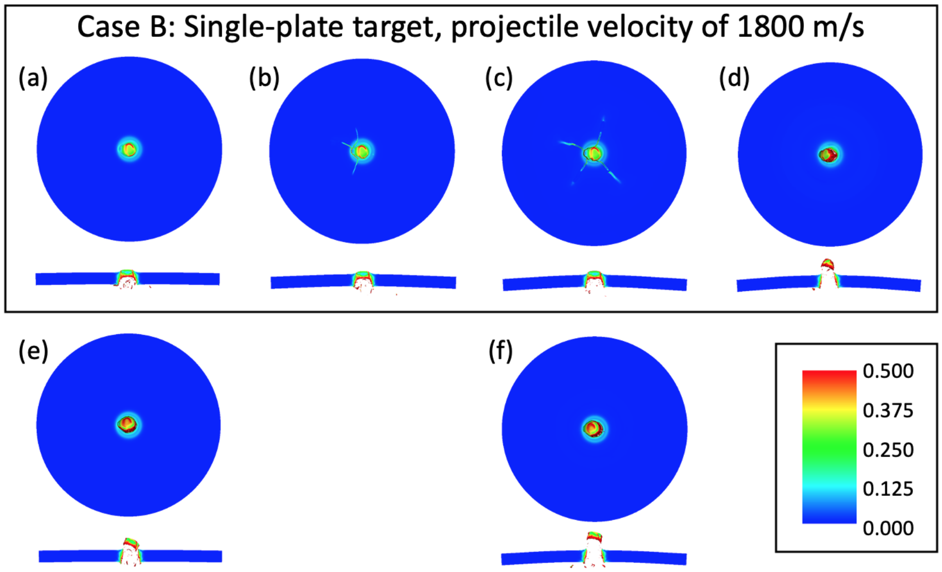

Fig. 4 Images at 90 μs showing effective plastic strain for a variety of 12.7-mm-thick plate (single-plate) configurations. A side-view slice and a rear view are included for each configuration with varying projectile velocity and explosive time delay: a) 1800 m/s, no explosive; b) 1800 m/s, 40-μs delay; c) 1800 m/s, 20-μs delay; d) 1800 m/s, 10-μs delay; e) 2000 m/s, no explosive; and (f) 2000 m/s, 20-μs delay.

Before continuing with cases A and B in more detail, a few comments regarding the explosive are necessary. The quantity of explosive was intentionally chosen to have a minimal effect on the target. For example, against a *single* 6.35-mm-thick rolled homogeneous armor plate (i.e., only one of the double-plate target plates) and at the same standoff distance, the model predicts a maximum effective plastic strain of 0.04. This strain value would hardly be visible using the same scale used in Figs. 3 and 4, with strains identified between 0.0 and 0.5.

The focus of this report now shifts to cases A and B, with the goal of understanding target failure. Enlarged images from case A are shown in Fig. 5. Detonation time delays of 10 and 5 μs result in crack-like failure (due to element deletion) of the rear target plate. Although increasing the detonation delay to 15 μs increases the plastic strain in the rear plate, there is no significant element deletion. A more quantitative expression of this behavior is shown in Fig. 6, which plots the maximum effective plastic strain observed in a slice taken through the middle of the rear target plate. Only the strain along a row of elements near the rear of the target plate was considered, and it is possible that there are other locations within the plate with higher effective plastic strains.

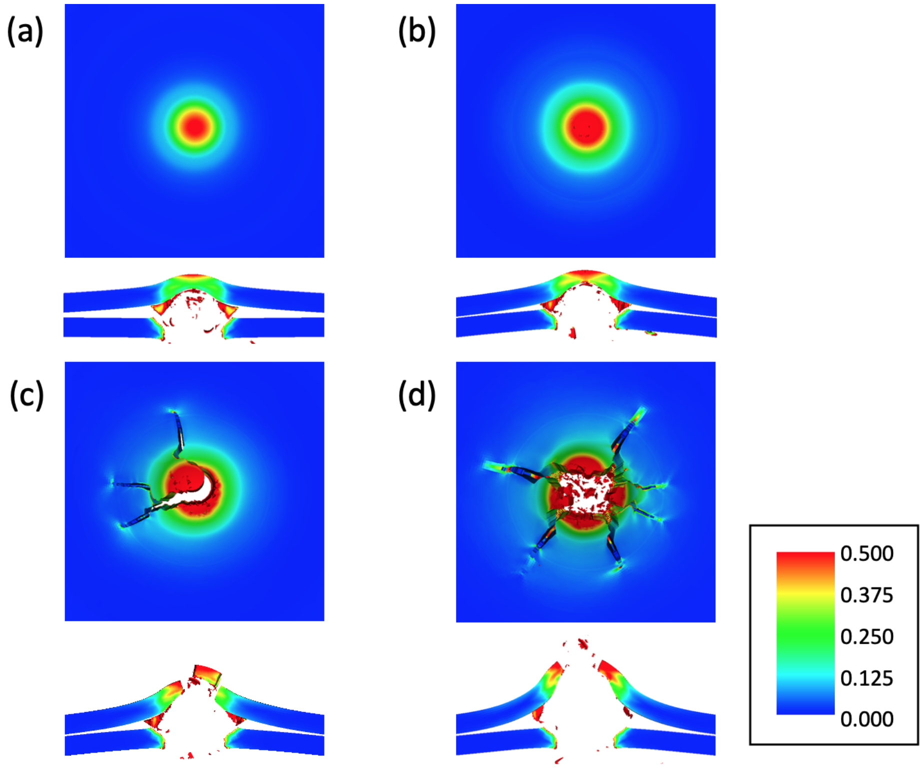

Fig. 5 Images showing effective plastic strain for case A (two 6.35-mm-thick RHA target plates with initial projectile velocity of 2000 m/s). This is an enlarged view of Figs. 3d–g showing an approximately 85-mm-wide region. The different configurations show variations in explosive time delay: a) no explosive; b) 15 μs; c) 10 μs; and d) 5 μs.

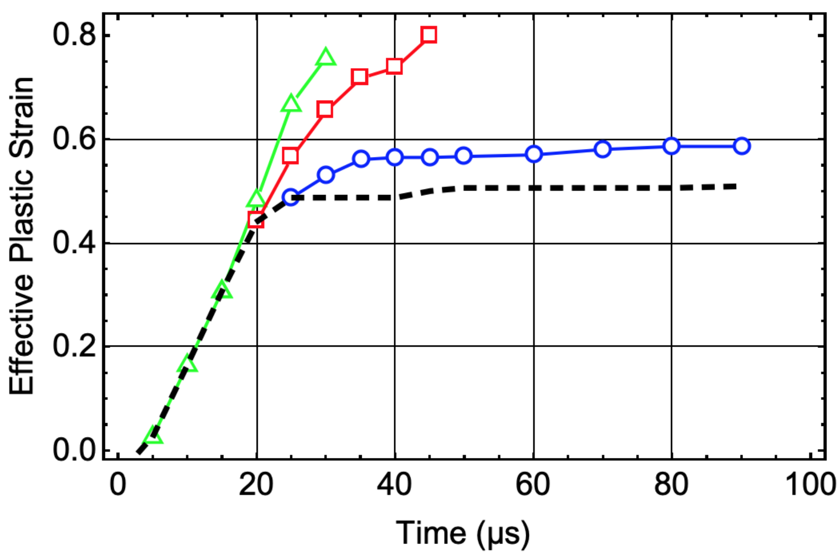

Fig. 6 Maximum effective plastic strain from a slice along the rear face of the rear plate (case A) is shown as a function of time for various detonation time delays: green/triangle—5 μs, red/square—10 μs, blue/circle—15 μs, and dashed black—no explosive

The plots in Fig. 6 highlight the differences between the 5- and 10-μs delays, compared to the 20-μs delay and the projectile-only case. The shorter time delays (5 and 10 μs) result in higher effective plastic strain and element deletion—strain was not plotted once elements were deleted, since the higher strain elements were no longer in the simulation. Deleted elements cause crack-like behavior as the plate material separates and opens as elements are removed. For the 20-μs delay, the strain reaches a limit value of approximately 0.58, which is higher than the projectile-only case ($\sim$0.5). The rear target plate still remains intact in both of these situations. One final thing to observe is that the differences in effective plastic strain for the various time delays, as shown in Fig. 6, first appear over a time interval of 15–25 μs.

Moving on to case B, enlarged images are shown in Fig. 7. In the vicinity of the impact region, the material state is very similar between the projectile-only case and the 40-μs-delay case. This is shown in Figs. 7a and b, although image b shows three distinct lines of localized strain emanating from the central region. For the 20-μs delay, these localized strain lines are longer and the strains are higher. In addition, plugging of the center region has begun with element deletion occurring along the left side of the plug circumference, relative to the image shown in Fig. 7c. As shown in Fig. 7d, with a shorter detonation time delay of 10 μs, the center has completely plugged out and there are no visible strain localization lines.

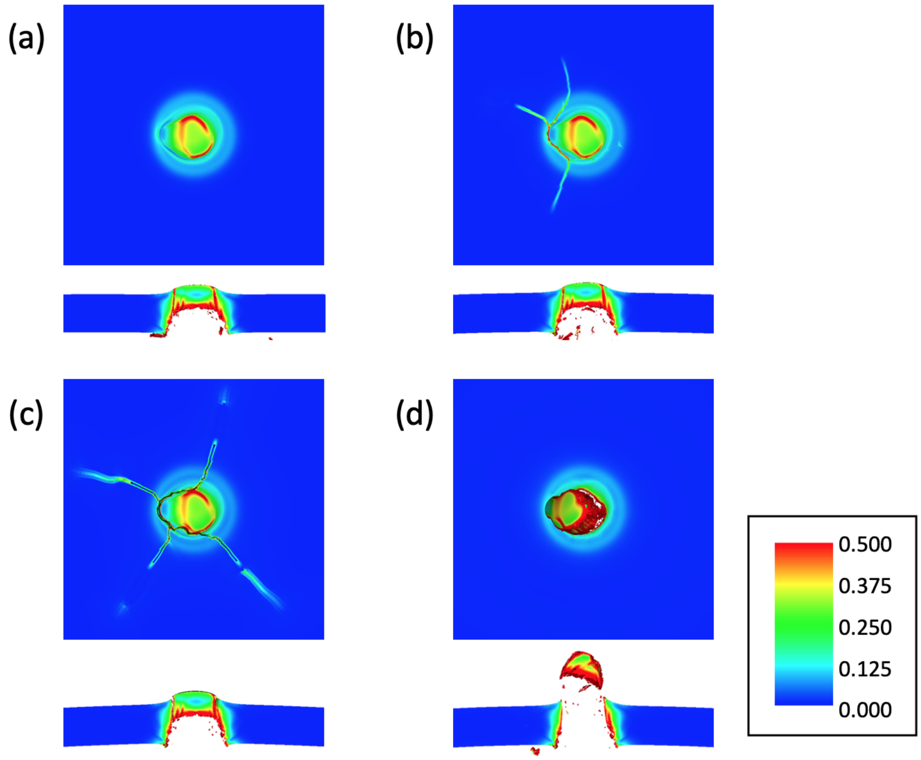

Fig. 7 Images showing effective plastic strain for case B (one 12.7-mm-thick RHA target plate with initial projectile velocity of 1800 m/s).This is an enlarged view of Figs. 4a–d showing an approximately 85-mm-wide region. The different configurations show variations in explosive time delay: a) no explosive; b) 40 μs; c) 20 μs; and d) 10 μs.

Figure 8 provides a more quantitative comparison between the four variations of case B. As mentioned with Fig. 6, the maximum strain values were obtained by considering elements taken from individual slices along the rear target face. This means that these values are not necessarily the overall maximum strains in the target, although they are representative of those strains and it is possible to see their evolution during the simulation from these plots. Both the projectile-only case and the 40-μs-delay case show the strain reaching a limit value without element deletion. This might also appear to be true for the 20-μs delay, but the drop in strain at 65 μs shows that element deletion has begun (i.e., the element with the highest strain at 60 μs is no longer in the simulation by 65 μs). Due to continual element deletion along a portion of the plug circumference, additional data was not recorded for the plot after 65 μs.

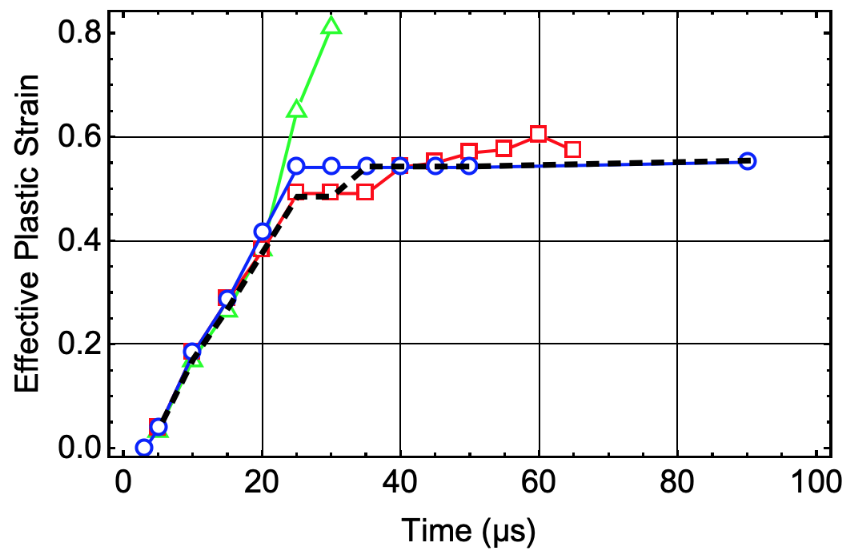

Fig. 8 Maximum effective plastic strain from a slice along the rear face of the target plate (case B) is shown as a function of time for various detonation time delays: green/triangle—10 μs, red/square—20 μs, blue/circle—40 μs, and dashed black—no explosive

Figure 8 also shows that, for the 10-μs-delay variant, the strain continues to increase as element deletion occurs in other areas of the target, leading to the complete separation (or plugging) of the central impact region. Differences in effective plastic strain for the 10-μs-delay case are first apparent between 20 and 25 μs. This time range is very similar to what was observed for the 5- and 10-μs delays with case A, as shown in Fig. 6.

After considering the effect of detonation time delays (Figs. 5 and 7) and visualizing the corresponding maximum strains (Figs. 6 and 8), four of the eight variants showed failure that included element erosion in the rear of the target.

- For three of these four variants, the failure initiated at times of less than 25 μs. The 5- and 10-μs delays with case A showed similar, and significant, cracking. The 10-μs delay with case B showed complete plugging.

- For the fourth variant (case B, with a 20-μs delay), failure begins after 50 μs. In this latter variant, there is partial plugging that is less severe than that for the corresponding 10-μs variant.

The remaining focus of this work considers these time and their relationship to failure initiation.

Figures 9 and 10 show the velocity of a node located on the rear face of the rear plate, near the center, for the case A variants. Tracking velocity allows one to observe when the blast first affects the rear of the target. This is seen by the deviation from the projectile-only plot at approximately 13.5 μs for the 5-μs-delay case, at 18.5 μs for the 10-μs-delay case, and at 24 μs for the 15-μs-delay case. The differences between detonation time and observed-effect time mean that it takes approximately 9 μs for the blast to affect the rear of the target. For case A, with the projectile traveling at 2000 m/s, it takes approximately 0.4 μs for the projectile to first contact the target (due to the 0.83-mm gap). Based on Fig. 10, the rear of the target is first affected at approximately 3.2 μs. By tracking a location on the rear face along the outer circumference of the rear target plate, the effect of the projectile impact is first observed at approximately 17.2 μs. This means that any reflecting waves from the free surface along the circumference would not reach the center until approximately 34 μs after the simulation has begun. (Since failure is not localized at the plate's center, it is more accurate to say that reflected waves would not reach the failed regions until 30–32 μs.)

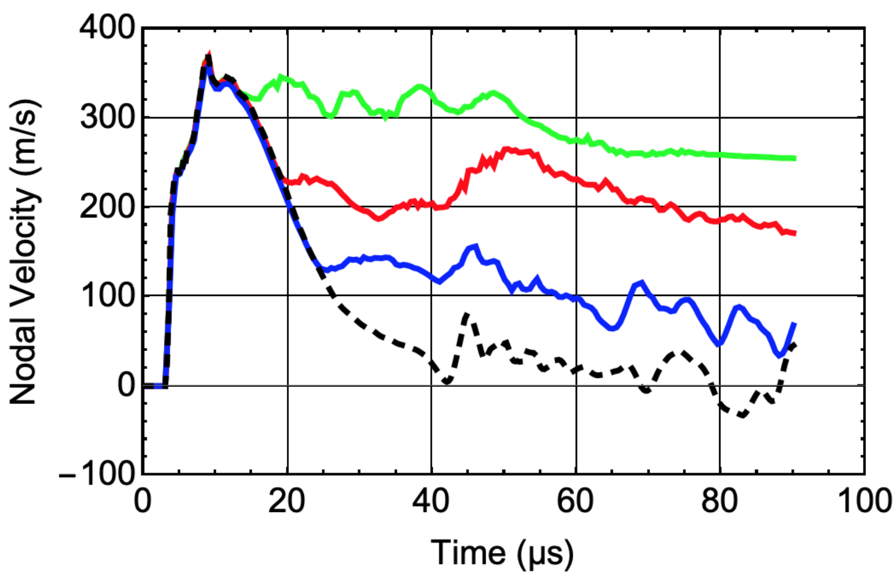

Fig. 9 Velocity near center of rear face of the rear plate (case A) is shown as a function of time for various detonation time delays: green—5 μs, red—10 μs, blue—15 μs, and dashed black—no explosive

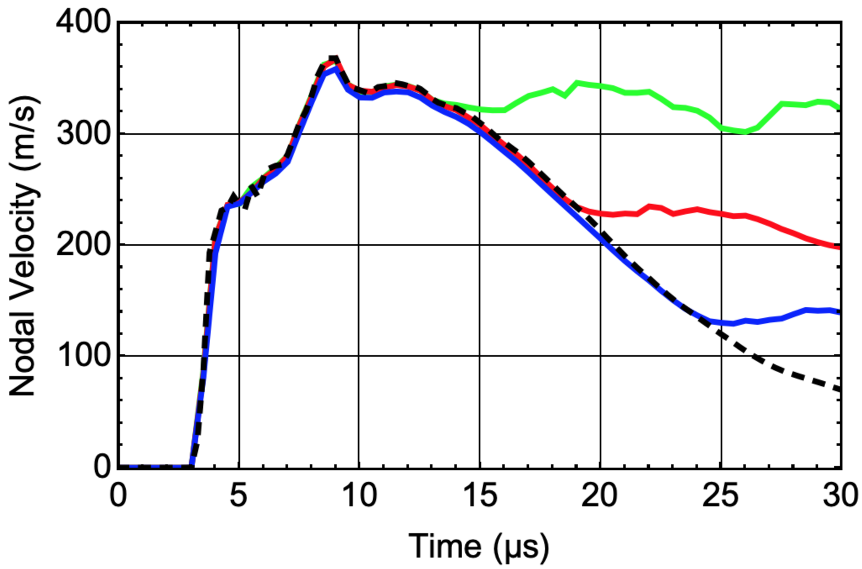

Fig. 10 Velocity near center of rear face of the rear plate (case A) is shown as a function of time for various detonation time delays: green—5 μs, red—10 μs, blue—15 μs, and dashed black—no explosive. This is the same data as shown in Fig. 9, but plotted over a shorter time range for added detail.

With these times in mind for case A, Fig. 11 shows the von Mises stress in an element located near the rear surface, toward the center of the rear target plate. The element yields very quickly after it is initially loaded, and the blast extends the time that the element yields (to over 40 μs for the 15-μs-delay variant). As a reminder, for the 5- and 10-μs detonation delays, failure occurs between an interval of 15–20 μs. This is the same time interval that yielding (without failure) occurs in the projectile-only variant. The time at which release waves would first reach the failed region (30–32 μs) occurs during the time of extended yielding due to blast, and so their effect is not visible in the von Mises stress plots. Also note that the element tracked in this figure does not fail and is not eroded. Depending on the explosive timing, this element's damage parameter, as used in the Johnson–Cook failure model, reaches a maximum value of between 0.15 and 0.23.

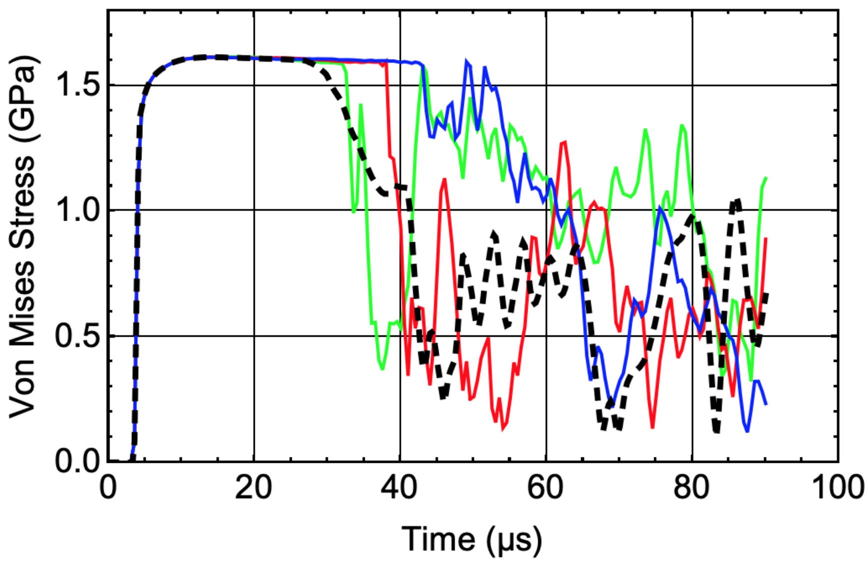

Fig. 11 The von Mises stress of an element located on the rear face of the rear plate (case A) as a function of time: green—5 μs, red—10 μs, blue—15 μs, and dashed black—no explosive

Figures 12 and 13 show rear-face velocities for case B (these figures correspond to Figs. 9 and 10 for case A). The case B, 10-μs-delay variant is discussed first, since it seems to be similar (in terms of timing) to the case A variants with failure. The blast effect is first noticeable at approximately 19 μs for the case B variant, which resulted in complete plugging. This difference (between 19 and 10 μs) means that there is a 9-μs interval between detonation and its effect on the rear of the target. The projectile for case B, traveling at 1800 m/s, takes approximately 0.5 μs to contact the target (due to the 0.83-mm gap) and the rear of the target is first affected at approximately 2.5 μs. Along the circumference of the target, at the rear face, the effect of the impact is first observed at approximately 17 μs, which is similar to the timing of case A. Therefore, any failure before 30–32 μs would not be affected by release waves from the free surface along the target edge.

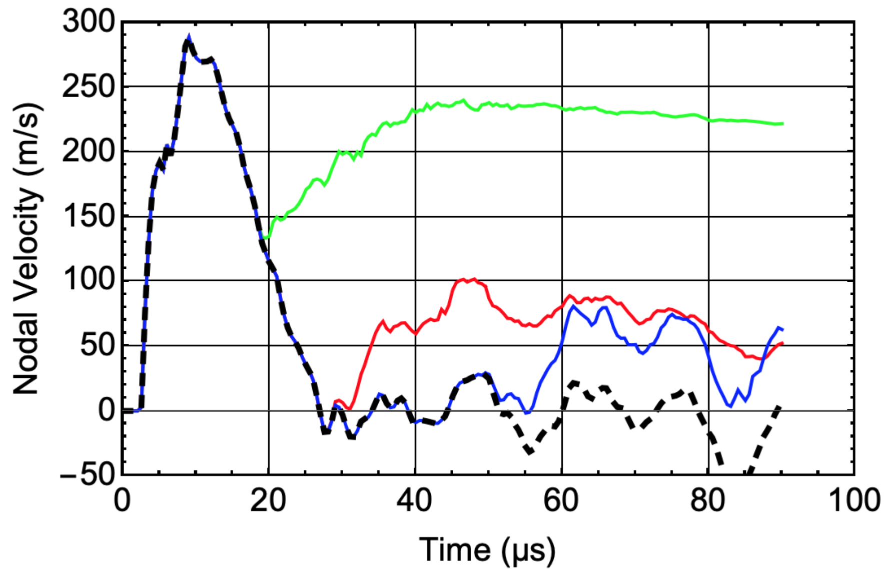

Fig. 12 Velocity near center of rear face of the target plate (case B) is shown as a function of time for various detonation time delays: green—10 μs, red—20 μs, blue—40 μs, and dashed black—no explosive

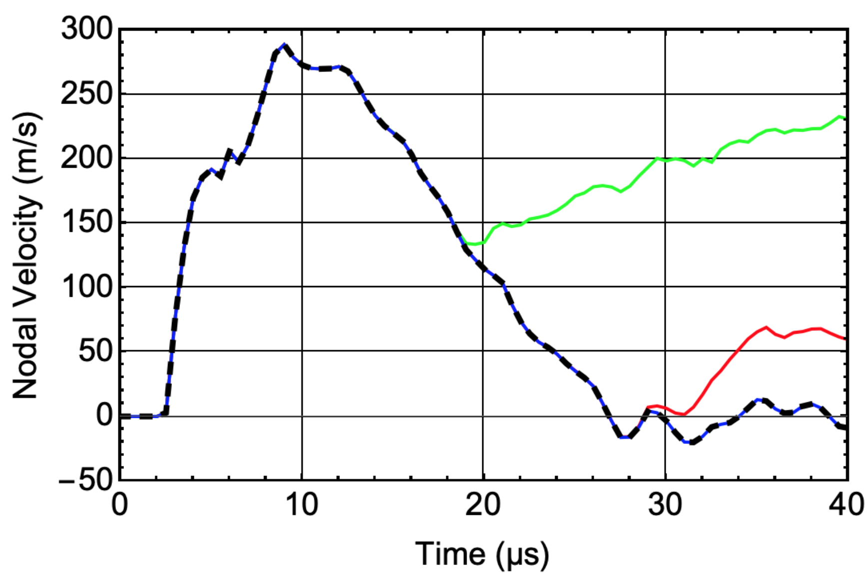

Fig. 13 Velocity near center of rear face of the target plate (case B) is shown as a function of time for various detonation time delays: green—10 μs, red—20 μs, blue—40 μs, and dashed black—no explosive. This is the same data as shown in Fig. 12, but plotted over a shorter time range for greater detail.

The final variant to consider is for the 20-μs delay for case B, where failure and erosion result in partial plugging and greater strain and damage localization compared with the 40-μs-delay case. The crack-like features are also longer for the 20-μs delay, as previously mentioned with Fig. 7c. As shown in Fig. 13, the blast effect is first noticeable at approximately 29 μs, although significant element erosion (associated with element failure) does not appear until after 50 μs. Also, since failure occurs after 30–32 μs, which is the time that release waves from the free edge would arrive back to the failure region, edge effects may influence the target's failure in this situation.

Figure 14 shows the von Mises stress of an element near the center of the rear surface of the target for case B. (This plot is similar to Fig. 11 for case A.) The 10-μs-delay case extends the region of yielding to nearly 30 μs, where significant element erosions have already occurred. For the 20-μs-delay case there is an increase in von Mises stress between 35 and 40 μs, compared with the projectile-only variant. However, it is difficult to notice any significant changes in the plotted stress values at times after 50 μs (when failure occurs). Just as with case A, the element tracked in Fig. 14 does not fail, nor does it erode. It reaches a maximum Johnson–Cook damage parameter of between 0.27 and 0.31, depending on the explosive detonation time. These values are larger than those from case A, with a corresponding range of 0.15–0.23.

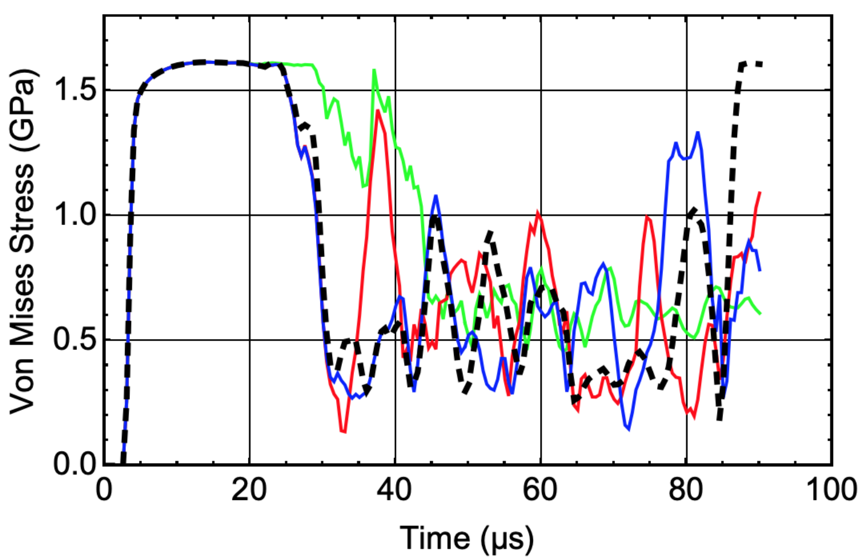

Fig. 14 The von Mises stress of an element located on the rear face of the target plate (case B) as a function of time: green—10 μs, red—20 μs, blue—40 μs, and dashed black—no explosive

4. Conclusions and Future Work

This work examined the combined blast-penetration effect in a highly idealized configuration using numerical modeling. The cases considered involved targets that were near their limit thickness (due solely to penetration) that could be pushed to failure by the addition of blast. The quantity of explosive was chosen to produce a blast that would, by itself, have very little effect on the the target.

Under these conditions, the relative timing between the penetration and the blast was found to be critical. In fact, major changes in target response were observed due to small changes in detonation time (e.g., less than 5 μs for the double-plate target system considered). These small changes in timing are of the same order of magnitude as the times associated with penetration, which are much shorter than those typically associated with blast-only interactions. For example, in three of the four cases that involved blast-induced failure, edge effects were not relevant due to the relatively early detonation times. Only for the fourth variant with failure did release waves from the free surface arrive at the failure region by the time of failure initiation.

To continue this work in the future, developing experiments capable of applying both penetration and blast loads would be very useful. The major experimental challenge will be the need to control the relative timing between the two load types. Using another type of penetrator may also be necessary to accommodate the combination of the two threat types in a single event.

Apart from experimental work, there are a number of additional modeling and simulations studies that could be conducted. Future efforts might consider the questions and topics listed as follows.

- Edge effects, even with the current target thicknesses and with the current projectile and explosive, could be studied by varying the target diameter.
- Are there more fundamental differences in combined-effect loading on single-plate versus multi-plate targets? Could this possibly explain the one variant (from this present study) that failed at a later time, compared with the other variants that failed?
- It might be useful to get a better sense of limit thickness and then to pro-

duce additional target and projectile configurations to analyze the relevant phenomena over a wider range of conditions (e.g., projectile speed, projectile shape, explosive mass).

- This work analyzed configurations near limit thickness for ballistic penetration, with minimal blast-only effect. A future study could consider the opposite case (i.e., near limit thickness for blast with the addition of a minimally effective projectile). One could also study cases between these extremes.

- A future study could try to separate the penetration and blast effect in time completely, by first subjecting a target to one threat and then later subjecting it to another. This would be easier to accomplish experimentally and it may provide a means of validating simulation results.

5. References

1. Rice MH, McQueen RG, Walsh JM. Compression of solids by strong shock waves. In: Seitz F, Turnbull D, editors. Advances in Research and Applications; (Solid State Physics; no. 6) Cambridge (MA): Academic Press; 1958. p. 1–63.

2. Johnson G, Cook W. A constitutive model and data for metals subjected to large strains, high strain rates and high temperatures. In: Proceedings of the 7th International Symposium on Ballistics; 1983 Apr 19–21; The Hague, The Netherlands. p. 541–547.

3. Meyer HW, Kleponis DS. Analysis of parameters for the Johnson-Cook strength model for 2-in-thick rolled homogeneous armor. Aberdeen Proving Ground (MD): Army Research Laboratory (US); 2001 June. Report No.: ARL-TR-2528.

4. Segletes SB. An examination of the JWL equation of state. Aberdeen Proving Ground (MD): Army Research Laboratory (US); 2018 July. Report No.: ARL-TR-8403.

5. Velodyne user's manual. ver. 4.003. Moorseville (NC): Corvid Technologies, Inc.; 2020 Mar.

1	DEFENSE TECHNICAL
(PDF)	INFORMATION CTR
	DTIC OCA
1	CCDC ARL
(PDF)	FCDD RLD DCI
	TECH LIB
2	CCDC GVSC
(PDF)	F RICKERT
	V BURGUESS

<u>ABERDEEN PROVING GROUND</u>

23	DIR CCDC ARL
(PDF)	FCDD RLW M
	B CHEESEMAN
	FCDD RLW PD
	B KRZEWINSKI
	A BARD
	N BRUCHEY
	R DONEY
	R GUPTA
	M KEELE
	D KLEPONIS
	K MASSER
	F MURPHY
	C RANDOW
	S SCHRAML
	K STOFFEL
	G VUNNI
	V WAGONER
	M ZELLNER
	FCDD RLW PE
	D HORNBAKER
	E KLIER
	C KRAUTHAUSER
	FCDD RLW PF
	N GNIAZDOWSKI
	C CUMMINS
	E FIORAVANTE
	S HUG